Fusion and Friction Stir Welding of Aluminum-Metal-Matrix Composites

D. STORJOHANN, O.M. BARABASH, S.S. BABU, S.A. DAVID, P.S. SKLAD, and E.E. BLOOM

Microstructure evolutions and degradations of aluminum-metal-matrix composites during fusion welding were studied and compared with thermodynamic calculations. In fusion welds of Al_2O_3-reinforced composites, the decomposition of Al_2O_3 was observed. In fusion welds of SiC whisker-reinforced composites, the decomposition of SiC to Al_4C_3 + Si by reaction with molten aluminum occurred. These phenomena led to unacceptable fusion welds in aluminum metal-matrix composites. Successful welds were produced in the same composites by friction stir welding (FSW). Significant reorientation of SiC whiskers close to the boundary of the dynamically recrystallized and thermomechanically affected zone (TMAZ) was observed. The small hardening in the dynamically recrystallized region was attributed to the presence of dislocation tangles in between SiC whiskers.

I. INTRODUCTION

THE joining of aluminum-metal-matrix composites is indeed a challenge, and limits the widespread application of these materials.[1,2] In the past, fusion welding, diffusion bonding, resistance welding, and friction welding have been used to evaluate the feasibility of joining these materials.[1–13] Among the fusion-welding processes, the arc, electron beam (EB), and laser beam (LB) methods have been considered, with and without filler wire. Resistance spot welding was performed, with and without a soft aluminum interlayer. Among the solid-state processes, capacitor discharge, friction, and diffusion bonding have been investigated before. Most of these investigations focused either on alumina (Al_2O_3)-reinforced composites[11,13] or on silicon carbide (SiC)-reinforced composites, in a wide range of cast- or wrought-aluminum alloys.[5]

It is generally known that the fusion-welding processes often leads to the deterioration of these metal-matrix composites. In the case of Al_2O_3-reinforced composites, the Al_2O_3 decomposes to aluminum and gas on contact with liquid aluminum.[13] Similarly, in the case of SiC-reinforced composites, the SiC reacts with molten aluminum to form Al_4C_3 carbide.[2] A review of the literature shows that the tendency toward the formation of Al_4C_3 can be reduced in certain arc-welding conditions.[13] During laser welding, it is very difficult to avoid these decompositions. However, Dahotre *et al.*,[4] in their elegant work, showed that decreasing the specific energy during laser melting could reduce the formation of Al_4C_3. Based on these two works and on other published research on Al-SiC composite welding, one can speculate that the tendency to form these Al_4C_3 carbides can be related to peak temperatures achieved in the melt, *i.e.*, a low specific energy leads to less superheating above the melting point of the aluminum alloy.

Therefore, in the first part of this research, the tendency to form carbides was evaluated with three different fusion-welding processes, and the weld-microstructure evolution was compared with the computational thermodynamic calculations. The autogenous fusion-welding processes were performed on two different aluminum-metal-matrix composites, *i.e.*, an Al-Al_2O_3 composite and an Al-SiC whisker composite. The tendency toward the degradation of the reinforcing particles was investigated, using optical microscopy and hardness.

It is also well established that friction- and capacitance-discharge-welding processes have more potential for joining these aluminum-metal-matrix composites.[10] There has been recent interest in the application of friction-stir-welding (FSW) processes to aluminum-metal-matrix composites.[14–18] Therefore, in the second part of this research, autogenous FSW was performed on Al-Al_2O_3 composites, as well as on Al-SiC whisker composites. The tendency toward particle degradation was investigated with optical microscopy and scanning electron microscopy (SEM). In addition, the tendencies toward reorientation of the SiC whiskers in different regions of FSW were examined with orientational imaging microscopy (OIM).

II. EXPERIMENTAL PROCEDURE

Two types of metal-matrix composites made by the casting method were used in this research. The first type is made with 20 vol pct reinforcing Al_2O_3 particulates, distributed in a 6061-alloy matrix. The alloy was in the solutionized condition. The nominal composition of the 6061 alloy is Al-0.6Si-0.28Cu-1.0Mg-0.2Cr (wt pct). The composite was provided by ALCAN International, USA. The samples were provided in sections that are 0.75 × 3 in. (19 × 76 mm) in size. The sections were then cut into small plates 4-mm thick. This sample will be referred as the Al-Al_2O_3 composite, throughout this article.

The second type of composite is made with a 20 vol pct silicon carbide (SiC) whisker distributed in a 2124 alloy matrix. The alloys were provided in the peak-aged condition.

D. STORJOHANN, Graduate Student, is with the Metallurgical and Materials Engineering Department, Colorado School of Mines, Golden, CO 80401. O.M. BARABASH, S.A. DAVID, P.S. SKLAD, and E.E. BLOOM are with the Metals and Ceramics Division, Oak Ridge National Laboratory, Oak Ridge, TN 37831. S.S. BABU, formerly with the Metals and Ceramics Division, Oak Ridge National Laboratory, is with the Edison Welding Institute, Columbus, OH 43017. Contact e-mail: suresh_babu@ewi.org

Manuscript submitted February 2, 2005.

The nominal composition of the 2124 alloy is Al-4.4Cu-0.6Mn-1.5Mg (wt pct). The 4-mm-thick plates were sectioned from a large plate. This sample will be referred as the Al-SiC composite throughout this article.

To evaluate the deterioration mechanisms of these composites under fusion-welding conditions, the plates were autogenously welded with gas tungsten arc (GTA), electron beam (EB), and Nd-YAG continuous wave laser beam (LB) welding processes. The welding process parameters were chosen to vary the energy density during the fusion-welding process. The heat input values used in these processes are as follows. The heat input during the GTA welding process was set at 4200 J/in. (165 J/mm). In the LB welding process, the heat input was set at 2750 J/in. (108 J/mm). In the EB process, the heat input was set at 150 J/in. (5.9 J/mm). The EB welding was performed in vacuum. Both the laser and arc welding were performed under argon shielding.

The FSW was performed on a milling machine, using a hardened tool steel pin. The rotational speed of the tool was 500 RPM and the translational speed was 2 in. per minute.

The welds were characterized by optical microscopy, SEM, OIM, and transmission electron microscopy (TEM). The hardness of the sample was measured, using the Vickers Hardness method with a 200-g force. To allow for the characterization of the SiC whiskers in the SEM, the samples were etched using an electrochemical method. The electrolytic solution was made with HNO_3 and methanol in a 1:2 ratio, respectively. The electrolytic etching was performed at 0 °C with 16 V for 2 minutes. This method allowed for the dissolution of the matrix to a depth that permitted the clear imaging of the SiC whisker orientation. The OIM was used mainly to evaluate the orientation of the SiC whisker in the base-metal (BM) and the friction-stir-welded region.

The TEM was used to analyze the microstructures of the Al-SiC composites in the friction-stir-welded region and in the heat-affected zone (HAZ). The samples for the TEM were produced using a standard ion-beam-thinning procedure. The TEM was performed using a PHILIPS* CM-12 transmission electron microscope.

*PHILIPS is a trademark of the Philips Electronic Instruments Corp, Mahwah, NJ.

III. THERMODYNAMIC CALCULATIONS

To evaluate the possible degradation of the aluminum-metal-matrix composites during the welding process, thermodynamic calculations were performed. The stable phases that can form at different temperatures were evaluated, using a nominal composition that averages the elemental contribution from the reinforcing particulate and the alloy matrix. The thermodynamic calculations were performed with ThermoCalc software[19] (ThermoCalc Software, Stockholm, Sweden), using the thermodynamic data from the solid-solution[20,21] and the pure-substance[20,21] database. The calculations were performed in an alloy system, Al-C-Cr-Cu-Mg-Mn-Si-O, and with the following phases: SiC, Mg_2Si, FCC, θ, Al_4C_3, $MgO.Al_2O_3$, Al_2O_3, and liquid. The calculations were performed as a function of temperature. The bulk composition of the Al-Al_2O_3 composite was calculated to be Al-0.15Cr-0.2Cu-0.73Mg-12.5O-0.44Si (wt pct). The bulk composition of the Al-SiC composite was calculated to be Al-6.86C-3.39Cu-1.16Mg-0.46Mn-16.0Si (wt pct). This bulk composition was calculated by adding the contributions from the alloy and the particulate whiskers.

IV. RESULTS

A. *Microstructure of Fusion Welds*

The optical microstructures of the fusion-welded Al-Al_2O_3 composites at different magnifications are shown in Figure 1. The BM microstructure shows no preferential alignment of the Al_2O_3 particulates, in either *x* or *y* directions. The notation of the *y* direction is taken along the thickness of the sample for convenience, and no significance is attached to this selection. The micrographs also show that the weld penetrations are small for all fusion-welding processes, including arc, EB, and laser (Figures 1(a), (d), and (g)). A comparison of the microstructures in the BM and the fusion zone (FZ) (Figures 1(b), (e), and (h)) shows the decrease in the volume fraction of the Al_2O_3 particulates. High-magnification micrographs from the FZ region of the arc and EB welds indicate clumping of the Al_2O_3 particulates. These clumped particulates also encircle large porosities (Figures 1(c) and (f)). In the laser welds, extensive dissociation of the original Al_2O_3 particulates can be observed (Figure 1(i)) in most of the weld-metal regions. The optical microstructures also show small black particles in the FZ region; the nature of these particles could not be resolved in this work. These results indicate that the fusion welding promotes the dissociation and clumping in Al-Al_2O_3 composites.

The optical microstructures of the fusion-welded Al-SiC composites in different magnifications are compared in Figure 2. All welds made on SiC-reinforced composites exhibit three distinct regions, *i.e.*, the FZ, the partially melted zone (PMHAZ), and the HAZ. In the micrographs, the boundary between the FZ and the PMHAZ is annotated as "FL," the fusion line. The boundary between the PMHAZ and the HAZ with porosities is annotated as "B1." The boundary between the HAZ and the BM region is annotated as "B2." The relative widths (Figures 2(a), (d), and (g)) of these regions (FL to B1; B1 to B2) varied with the different processes. The HAZ microstructure shows some evidence of porosities. The shapes and sizes of these porosities change from location to location in the HAZ. Most of the porosities are elongated along the *x* direction. It is speculated that this could be due to the interaction of the SiC whisker orientation and the direction of the principal tensile stresses that develop during weld heating and cooling. Further work is necessary to validate this speculation with detailed computational thermomechanical modeling. In the PMHAZ (Figures 2(b), (e), and (h)), the SiC whiskers appear to be intact; only the melting of the aluminum alloy can be seen. In the FZ (Figures 2(c), (f), and (i)), the SiC whiskers have completely dissolved during heating and have formed a complex microstructure during cooling. The Al_4C_3 needles, gray-faceted Silicon phase, and dendritic microstructures were observed. This microstructure was prevalent in all fusion welds, including GTA, EB, and LB welds. It is interesting that the laser welds showed deeper penetration, even though the heat input was lower than that of the GTA welds. This is associated with the greater absorption coefficient of laser radiation by SiC.[5,6]

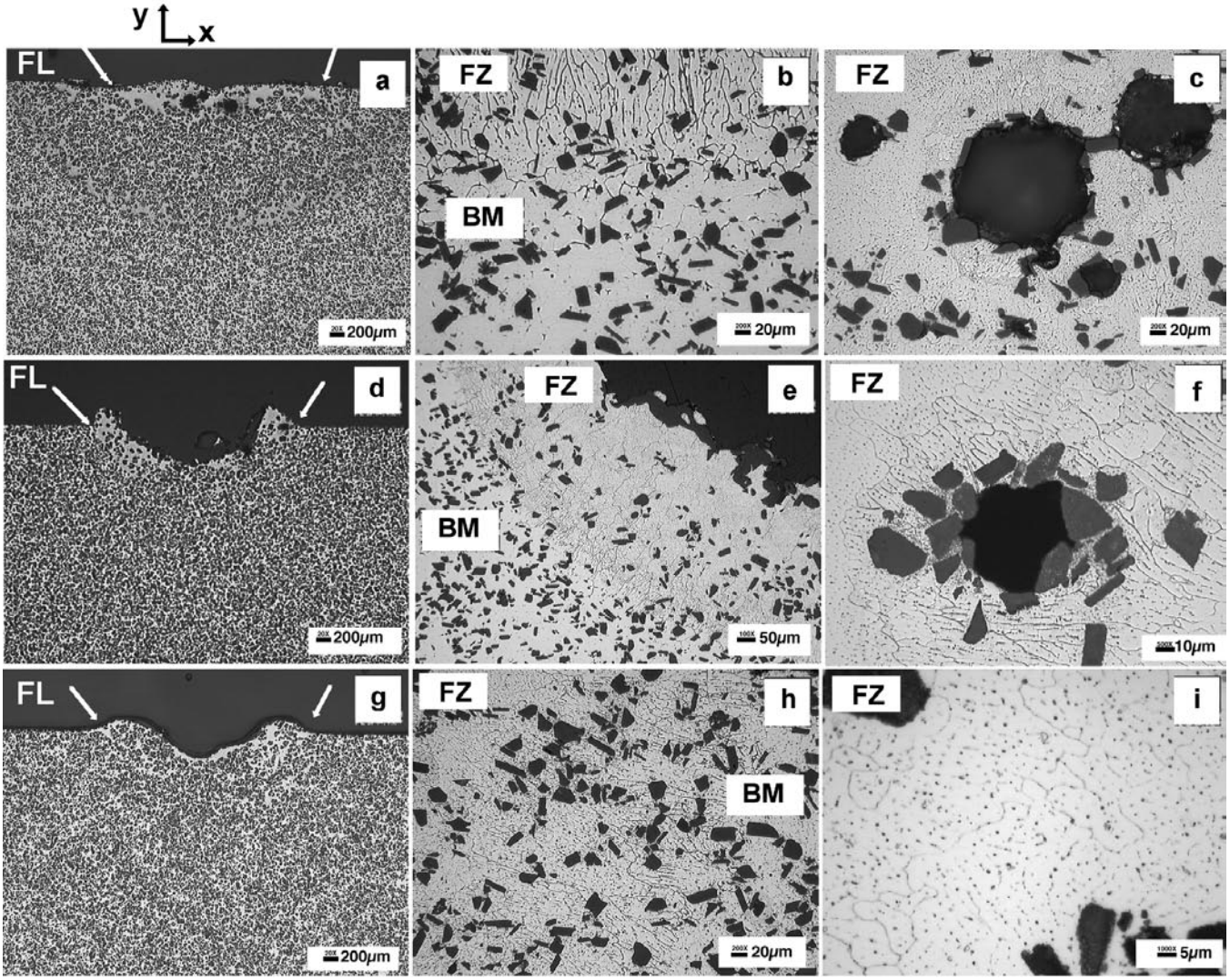

Fig. 1—Optical micrographs of fusion welds made with different welding processes on Al-Al_2O_3 composites are compared: (*a*) through (*c*) the GTA welds, (*d*) through (*f*) the EB welds, and (*g*) through (*i*) the LB welds. The arrows indicate the approximate fusion line locations. The directions *x* and *y* are in the plane of the micrographs, and the *z* direction perpendicular to the *x*-*y* plane is the welding direction.

The hardness measurements from all the fusion welds are compared in Figure 3. The hardness of the Al-Al_2O_3 composite BM is slightly softer (100 to 140 HV) than that of the Al-SiC composite (180 to 190 HV) BM. The BM and HAZ regions occasionally exhibit large hardness, due to the preferential sampling of a large volume fraction of reinforcements. These variations are smaller in Al-SiC composites than in Al-Al_2O_3 composites. These variations are related to differences in the size of the particles in the composites. The Al_2O_3 particles (~20 μm) are coarser the SiC whiskers (~1 to 2 μm in diameter and 5 to 7 μm in length). As a result, occasionally, during hardness measurements, large fractions of Al_2O_3 particles may be sampled, which leads to large variations. As expected, the FZ region of the Al-Al_2O_3 composites is softer (Figure 3(a)) than the BM region. This is associated with the removal and clumping of the Al_2O_3 particles in the FZ region. In the case of Al-SiC composites, the FZ region is harder than both the HAZ and BM regions. This is attributed to the formation of hard Al_4C_3 phases in the FZ region.

B. *Microstructure of Friction Stir Welds*

Successful joints were made in both composite materials with FSW processes. The microstructures from different regions, from both the Al-Al_2O_3 and Al-SiC composites, are presented here.

The BM microstructures from the Al-Al_2O_3 composites show the presence of angular Al_2O_3 particles ~20 μm in size (Figure 4(a)). The macrostructure showed three distinct regions: the HAZ, the TMAZ, and the directionally recrystallized region (DXZ), in the middle of the joint. The microstructure from the BM and the HAZ did not show any major differences. The microstructure from the TMAZ showed some evidence of Al_2O_3 particle breaking, which was indicated by the presence of smaller particles (Figure 4(b)). In addition, there appears to be segregation of these small particles, which gives rise to the formation bands. Compared to the BM, the DXZ region did not show significant differences in coarse particulate distributions (Figure 4(c)), except for the appearance of small particles. The

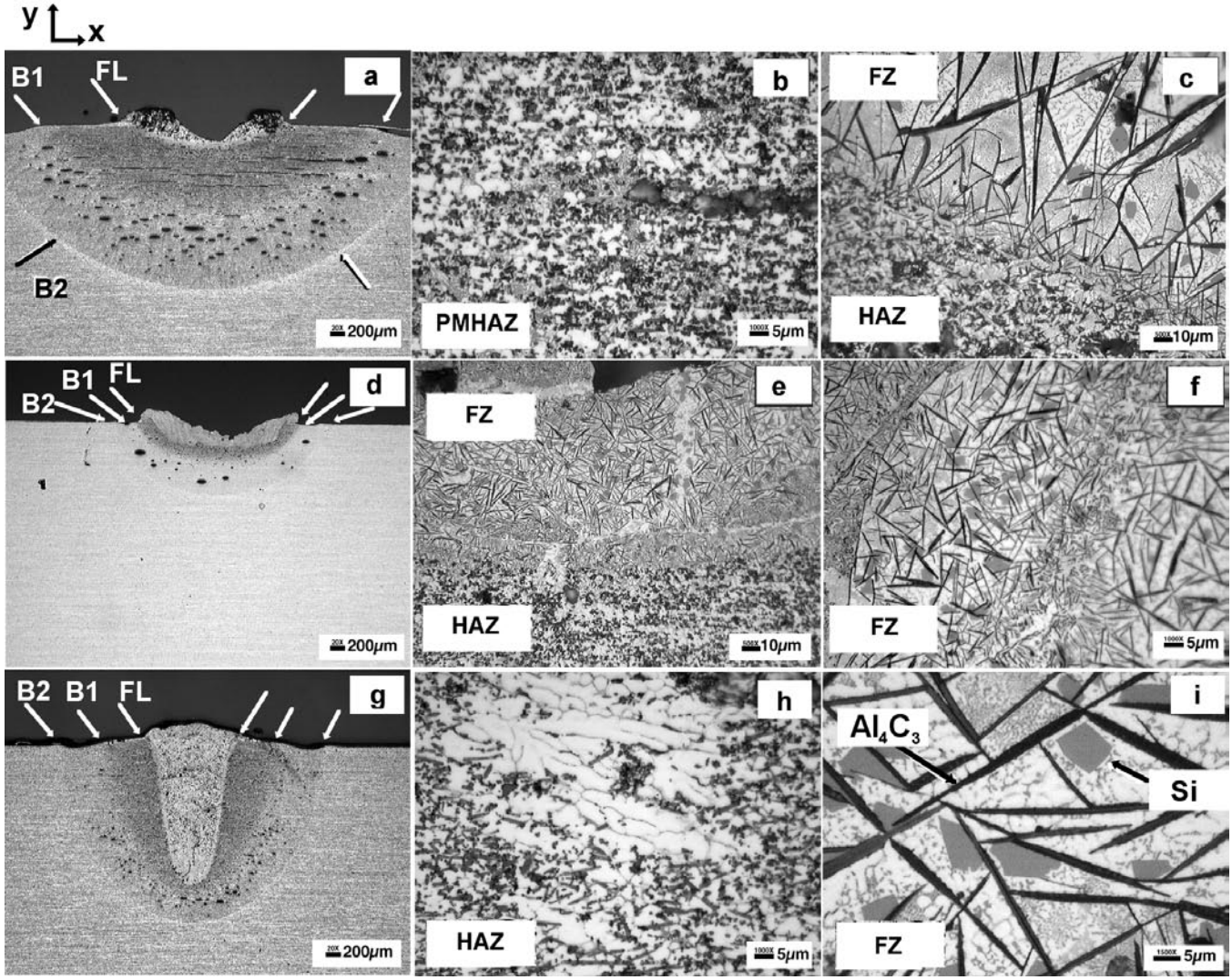

Fig. 2—Optical micrographs of fusion welds made with different welding processes on Al-SiC composites are compared: (*a*) through (*c*) the GTA welds, (*d*) through (*f*) the EB welds, and (*g*) through (*i*) the LB welds. The needlelike features in (*c*), (*f*), and (*i*) are aluminum carbides, and the gray-colored angular precipitates are silicon phase. The fine mottled structure is eutectic constituents formed during the later stages of weld solidification. Arrows mark the approximate locations of the FL, B1, and B2. The directions *x* and *y* are in the plane of the micrographs, and the *z* direction perpendicular to the *x*-*y* plane is the welding direction.

discussion of particle breakage in both the TMAZ and the DXZ region will be presented in Section V. The hardness measurements across the DXZ, TMAZ, HAZ and BM regions are shown in Figure 5. The hardness measurements from the DXZ and the BM region were similar (100 to 140 HV). In the TMAZ regions, the occasional clustering of the Al_2O_3 particles led to a large increase in hardness (>200 HV), which is evident in Figure 5.

The comparisons of the microstructures from different regions, in the case of the Al-SiC composites, are given in Figure 6. The BM microstructure (Figure 6(a)) shows the presence of whiskers in different orientations. Cursory analyses showed that the orientation of the SiC whiskers was mostly along the *x* direction in the base material, due to the original processing done on these composites. The microstructure from the DXZ region (Figure 6(c)) is similar to that of the BM region, with a small tendency toward the clustering of the whiskers, as marked by the series of arrows. In the TMAZ/DXZ boundary regions (Figure 6(b)), there is apparent alignment of the major axes of the SiC whiskers along the welding direction. This phenomenon is analyzed further with SEM.

To allow for the clear observation of the SiC whisker orientations in the different regions of the Al-SiC friction-stir-welded samples, electrolytic etching was used to preferentially remove the matrix layers. The scanning electron micrographs from the DXZ region in the middle of the joint, at different magnifications, are shown in Figures 7(a), (b), and (c). The micrographs show the presence of hexagonal whiskers in two different orientations. The major axes of many of the whiskers are aligned along the *x* direction. Other whiskers are aligned perpendicular to the *x*-*y* surface, along the *z* direction. Micrographs at high magnification do not show much difference in the SiC whisker orientations between the DXZ and the BM regions (Figures 7(a), (b), (e), and (f)). The SiC whisker orientations near the boundary of the TMAZ and DXZ on the left side (Figure 7(d)) and on the right side of the joint (Figures 7(g) and (h)) show

clear evidence of the aligning of almost all the SiC whiskers along the welding direction (*z* direction). It is important to note that, at this boundary, the metal flow is also along the welding direction (*z* direction).

Additional analysis of the SiC whisker orientation was performed by observing the microstructure at different locations, starting from the DXZ region and traversing across the boundary to the BM region, as shown in Figure 8. The microstructures clearly show the gradual change in SiC orientations, *i.e.*, near the surface in the DXZ region (Figure 8(a)), most of the SiC whiskers from the DXZ are aligned along the *z* direction. In contrast, in the BM (Figure 8(f)) close to the bottom of the joint, the orientations are mostly along the *x* direction. This result shows that FSW of Al-SiC composites leads to a substantial reorientation of the SiC whiskers, due to the material flow.

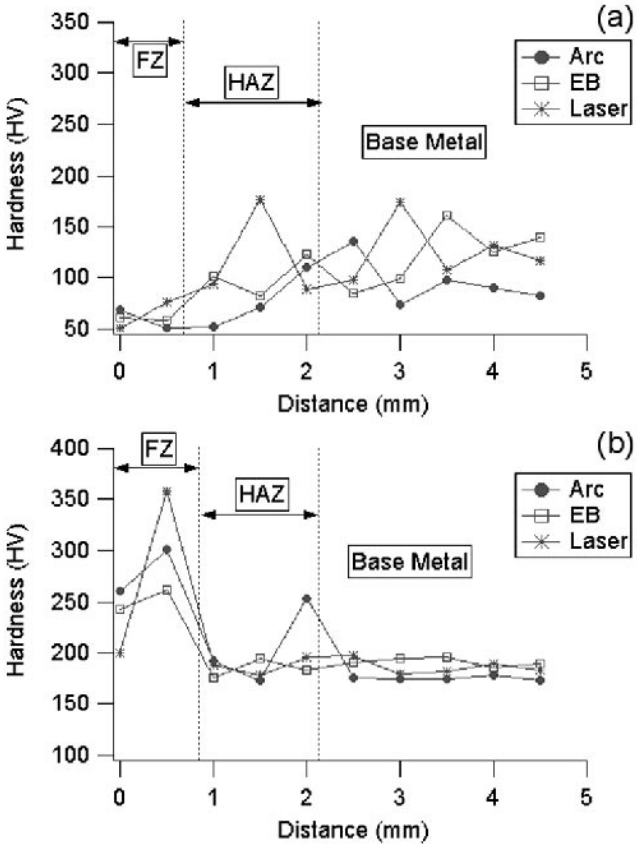

Fig. 3—Measured hardness values across the fusion weld made on (*a*) Al-Al_2O_3 composites and (*b*) Al-SiC composites, as a function of distance with different processes. The FZ region of the Al-Al_2O_3 composites is softer, due to dissociation of the Al_2O_3. The FZ region of the Al-SiC composites is harder, due to the formation of the Al_4C_3 phase.

In order to quantify these orientation differences in the SiC, OIM was performed on these samples in the BM region, in the boundary between the TMAZ and the DXZ, and also in the DXZ. The OIM analyses identified two forms of SiC, *i.e.*, close-packed hexagonal (alpha) and cubic form (beta). Since the majority of the phase is hexagonal form, the alpha form of the SiC was considered for further analyses. The orientational imaging microstructures and their respective textures from these regions are compared in Figure 9. It is important to note that the measurements are approximate, since the surfaces of the samples are not perfectly flat, due to the etching technique used. The {0001} textures from the BM (Figure 9(a)) and the DXZ (Figure 9(b)) show a similar configuration, except for a small rotation. In contrast, the measurements from the boundary regions (Figure 9(c)) show a large {0001} rod texture. This result substantiates the qualitative observation of the SiC whisker orientation differences in the scanning electron micrograph shown in Figure 7. This preferential alignment of the SiC whiskers is attributed to the direction of the metal flow during FSW.

The measured hardness across the joint region (Figure 10(a)), showed that the DXZ regions (170 HV) are slightly softer than the BM (Figure 3(b)) regions (170 to 190 HV). The TMAZ and HAZ regions (133 to 160 HV) were slightly softer than the DXZ region. Furthermore, the spatial variations of hardness measured using the automated indenter testing apparatus are shown in an image format in Figure 10(b). The results show that the hardness variations within the DXZ are not uniform. These spatial heterogeneities are attributed to differences in the metal flow in different locations.

The typical microstructure in between the SiC whiskers in the aluminum matrix was investigated using TEM (Figure 11). The matrix from the DXZ regions (Figure 11(b)) showed a large concentration of dislocations and dislocation networks. In contrast, the matrix regions in the HAZ (Figure 11(a)) showed a highly recovered structure. It is important to note

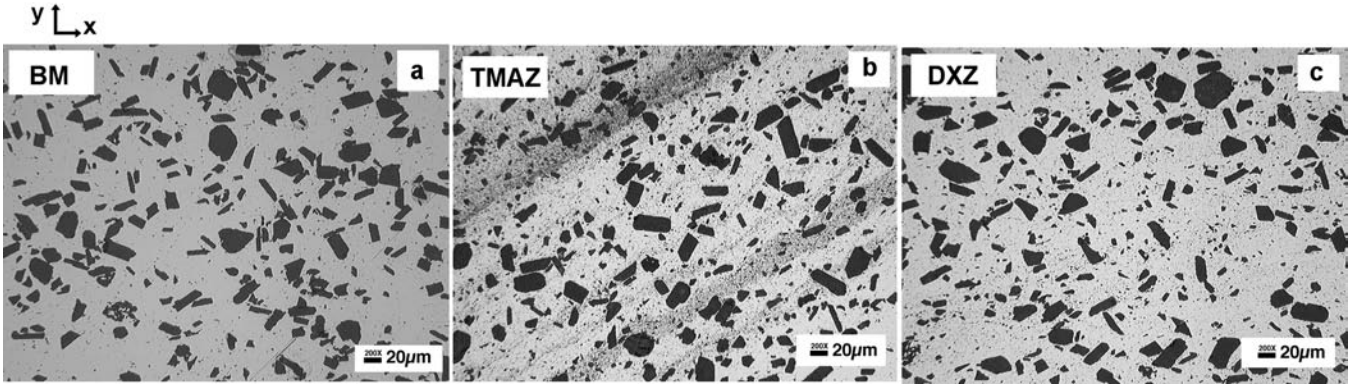

Fig. 4—Optical micrographs of the friction stir weld made on Al-Al_2O_3 composites are compared: (*a*) the BM region, (*b*) the TMAZ region, showing the bimodal nature of particles, with small particles being segregated along bands, and (*c*) the DXZ region, showing the presence of both coarse and fine particles. The directions *x* and *y* are in the plane of the micrographs, and the *z* direction perpendicular to the *x*-*y* plane is the welding direction.

that these observations are typical and do not represent the overall region. To allow for the study of the dislocation content and the tendency to form subgrain boundaries in a wide range of areas, either Laue or Synchrotron diffraction methods are needed.[22,23] This will be the focus of future work.

V. DISCUSSION

The results described in Section IV show that the fusion welds most often lead to the deterioration of the aluminum-metal-matrix composites. In contrast, the friction stir welds can produce good joints, with small changes to the characteristics of reinforcements. In this section, possible degradation mechanisms in both friction and fusion welds are discussed.

A. *Deterioration of Reinforcements in Fusion Welds*

The current work and other published works clearly show that the fusion welds is not suitable for the joining of metal-matrix composites. In the case of Al-Al_2O_3 composites, the dissociation of Al_2O_3 occurs. In case of Al-SiC composites, the reaction between the SiC and the molten liquid leads to the formation of brittle Al_4C_3 carbide. Earlier work by Ellis *et al.*[13] showed that, under certain conditions of the GTA welding process, the deterioration of SiC could be avoided. This shows that the energy density plays an important role in the deterioration of reinforcements. In addition, other work has shown that, even in laser welds with a high energy density,[4,24] pulsing will reduce the tendency toward the formation of carbides. Since the peak temperature of the molten pool is related to the energy density, one can envision that the deterioration is directly linked to the temperatures achieved in the weld pool. To evaluate that hypothesis, one could evaluate the phase stability of these reinforcements as a function of composition and temperature. In the past, Devletian[12] used the standard free-energy estimates to describe the formation of Al_4C_3 carbides. Zheng and Reddy used thermodynamic calculations to study the stability of different reinforcements under casting conditions.[25] Others have used similar approaches to design the interfaces between the composites and the aluminum matrix.[26] In the current work, we evaluated the stability of different phases as a function of superheating above the melting point of aluminum, using computational thermodynamic models.

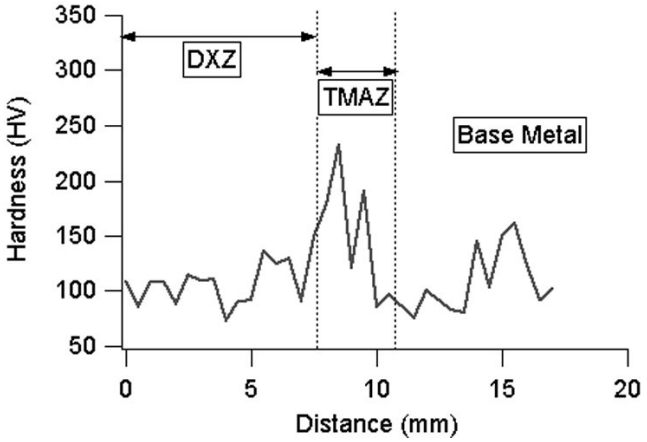

Fig. 5—Measured hardness values across the friction-stir-welded joint. The hardening in the TMAZ region corresponds to the possible clustering of Al_2O_3 particles, similar to Figure 4.

The predicted mole fractions of various phases for Al-Al_2O_3 composites as a function of temperature are shown in Figure 12(a). The calculations show that, on exposure to molten aluminum, the Al_2O_3 does not decompose below 2000 K. However, above 2000 K, the evaporation of molten aluminum coincides with the dissociation of Al_2O_3. It is important to note that, in these calculations, the thermodynamic data assumes that there is very little solubility of oxygen in the molten aluminum. This is, indeed, consistent with the work by Zheng and Reddy.[25] This is the reason for the extended stability of Al_2O_3 in the molten aluminum. The formation of porosities very close to the surface of the weld pool is attributed to the generation of a high temperature during welding in the arc, EB, and laser welding processes. An additional factor that controls the weld penetration is the presence of Al_2O_3 in the molten aluminum liquid, which may increase the viscosity of the liquid and, therefore, cut down the convective flow.[13] This, in turn, will stifle the formation of the weld pool, which is evident in this work. The calculations shown in Figure 12(a) indicate that the deterioration of Al_2O_3 below the liquidus temperature will be very minimal.

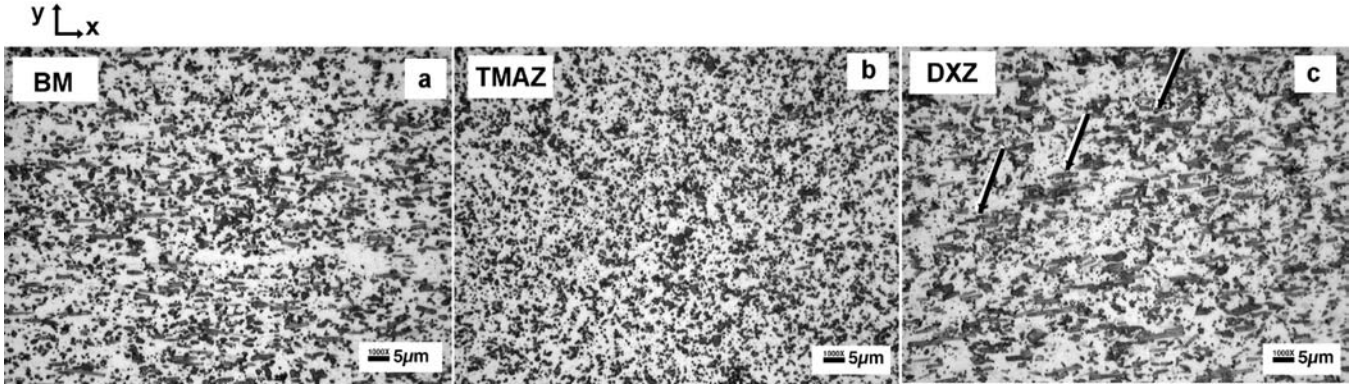

Fig. 6—Optical micrographs from different regions of the friction stir weld made on the Al-SiC composites are compared: (*a*) the BM region, (*b*) the TMAZ region, and (*c*) the DXZ region. An apparent change in the SiC orientation can be observed in Fig. 6(b). The series of arrows in Fig. 6(c) indicates the apparent clustering of SiC whiskers. The directions *x* and *y* are in the plane of the micrographs, and the *z* direction perpendicular to the *x*-*y* plane is the welding direction.

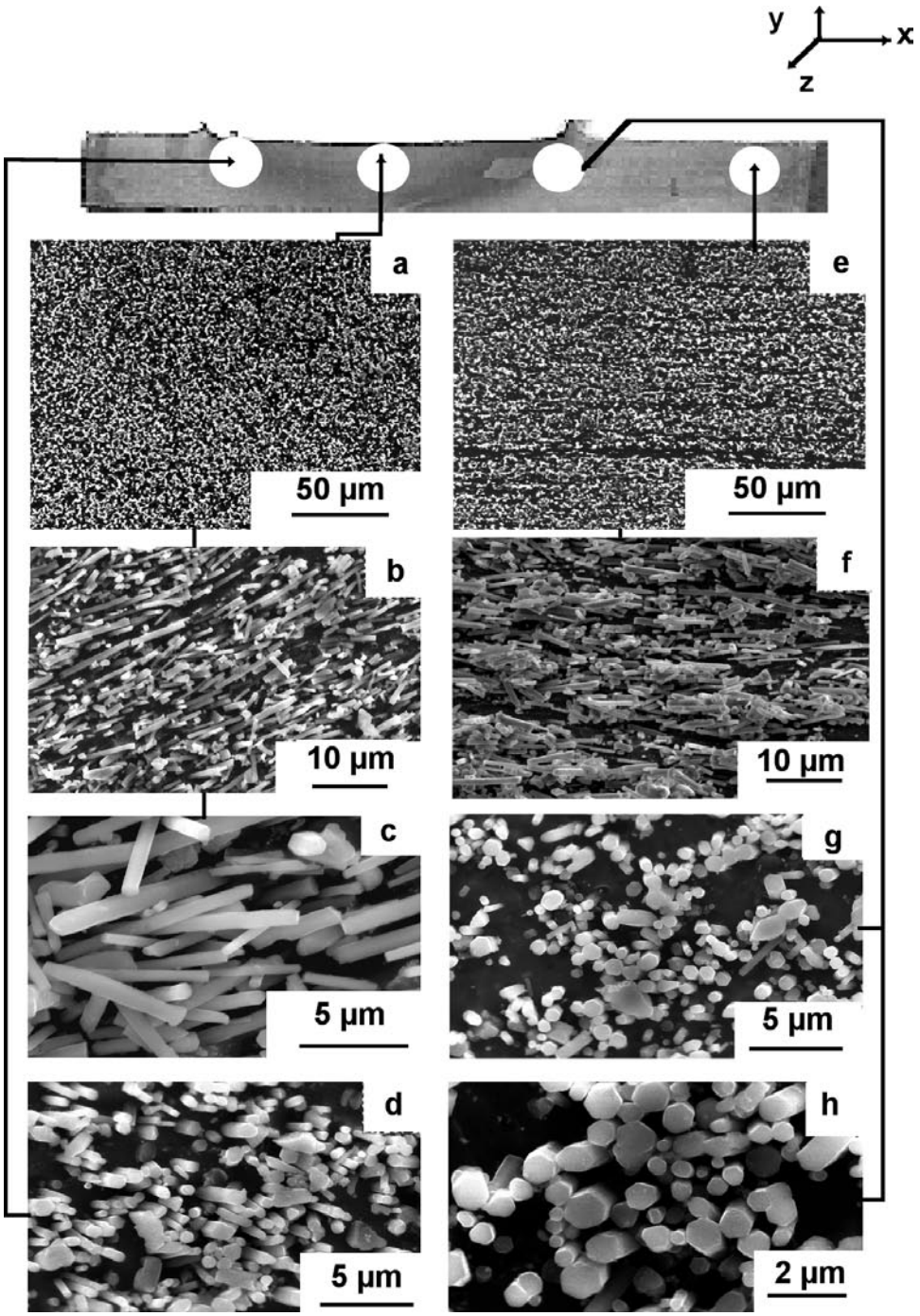

Fig. 7—Secondary electron images from the deeply etched transverse section of the friction-stir-welded Al-SiC composites, showing different spatial orientations of the SiC whiskers: (*a*) through (*c*) the DXZ region, (*d*) the left-side boundary between the TMAZ and DXZ regions, (*e*) through (*f*) the BM region, and (*g*) and (*h*) the right-side boundary between the DXZ and the TMAZ. The *x* and *y* direction are on the plane of the micrographs, and the *z* direction is out of the paper and perpendicular to the surface of the micrographs and along the welding direction.

The predicted mole fractions of the various phases for Al-SiC composites as a function of temperature are shown in Figure 12(b). The calculations indicate that, as soon as the temperature exceeds the melting point of aluminum, the reaction between the SiC and the molten aluminum is triggered to form the Al_4C_3. It is interesting that the extent of this reaction slowly increases from the melting point of the aluminum and reaches complete displacement of the SiC at ~2000 K. This suggests that it is possible to retain a large amount of SiC by reducing the superheating of molten aluminum. For example, one can achieve low superheat by using the GTA welding process. If the superheat is low, the displacement reaction may be limited to the interface between the molten aluminum and the SiC. This was, indeed, reported in the work by Ellis *et al*., where the reaction layer was reported only close to the SiC particulate. In contrast, the formation of Al_4C_3 was observed in the current arc welding conditions. Ellis *et al*. used heat input ranges from 900 to 1740 J/mm to

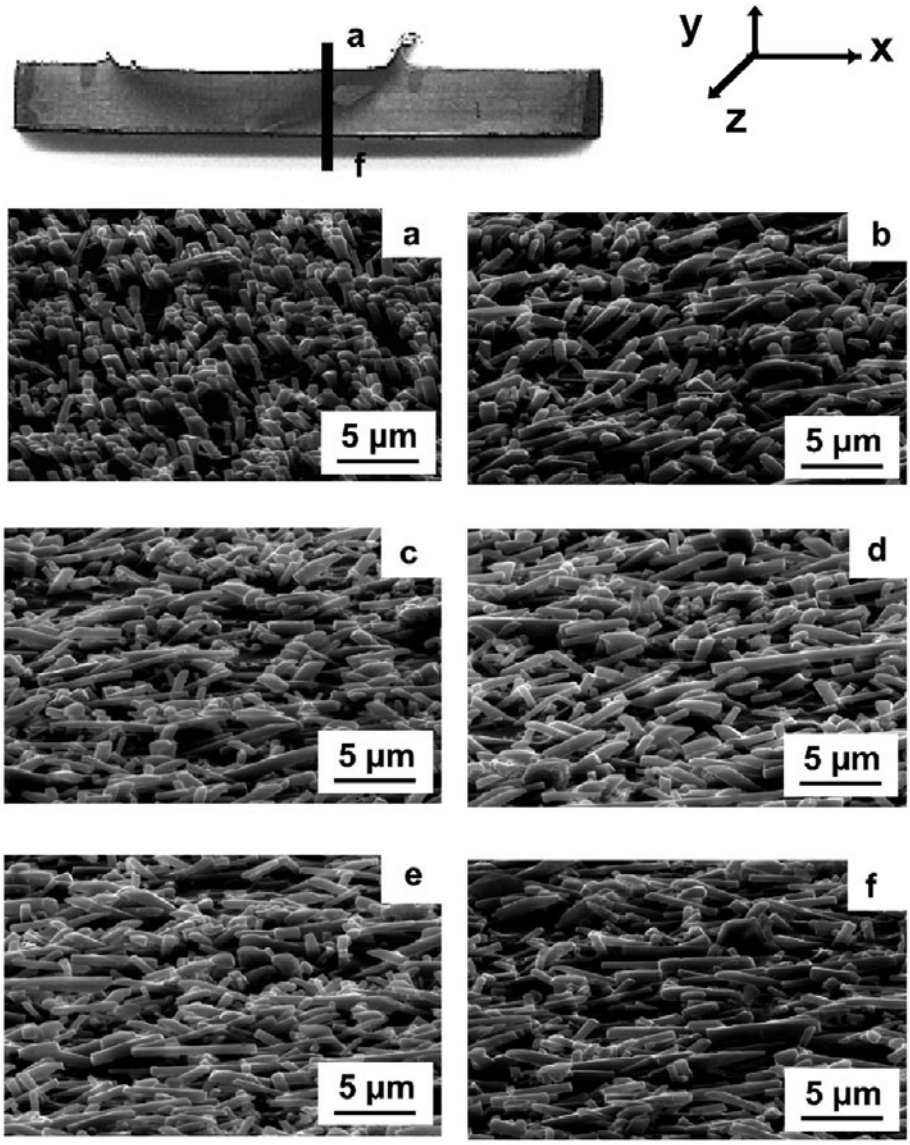

Fig. 8—Secondary electron images from the deeply etched transverse section of the friction-stir-welded Al-SiC composites, showing different spatial orientations of the SiC whiskers as a function of depth from the top surface (in the DXZ region, close to the TMAZ boundary) to the bottom surface (the BM region). The *x* and *y* direction are on the plane of the micrographs, and the *z* direction is out of the paper and perpendicular to the surface of the micrographs and along the welding direction.

achieve weld-pool widths from 6.5 to 9 mm and weld-pool depth of penetration from 1 to 3 mm, respectively. Assuming a simple rectangular geometry, these values correspond to an energy-density-per-unit volume in the range of 140 to 64 J/mm^3. In the present experiments, the heat input used in the GTA welding process was 165 J/mm, the width of the weld pool was approximately 2 mm, and the depth of penetration was 400 μm. This corresponds to an approximate energy density of 206 J/mm^3. This shows that, in the current research, the energy density of the GTA welding process is at least twice that of the welding processes used by Ellis *et al*.[13] As a result of the higher energy density in the current arc welds, the molten metal could have experienced higher superheat, which would have induced extensive decomposition of the SiC to Al_4C_3. The current results, in conjunction with the results by Ellis *et al*.[13] and Dahotre *et al*.,[4] suggest that it is possible to control the decomposition of SiC by carefully managing the superheat in the melt, either by using pulsed arc welding or pulsed laser welding processes. Alternatively, one could use the approach suggested by Zheng and Reddy[25] to alloy the weld-pool region with titanium, which will trigger the formation of titanium carbide instead of aluminum carbide. Zheng and Reddy[25] also suggested the *in-situ* formation of nitrides or oxides for the casting conditions, by deliberate alloying with Ti or Zr. However, they also stress the need to control the temperature of the molten metal.

B. *Deterioration of Reinforcements in Friction Stir Welds*

In this section, possible degradation mechanisms for reinforcements in both Al-Al_2O_3 and Al-SiC composites are discussed.

Although the optical microstructure (Figure 4) of the Al-Al_2O_3 composites showed no significant differences, there was some systematic increase in the number of smaller particles

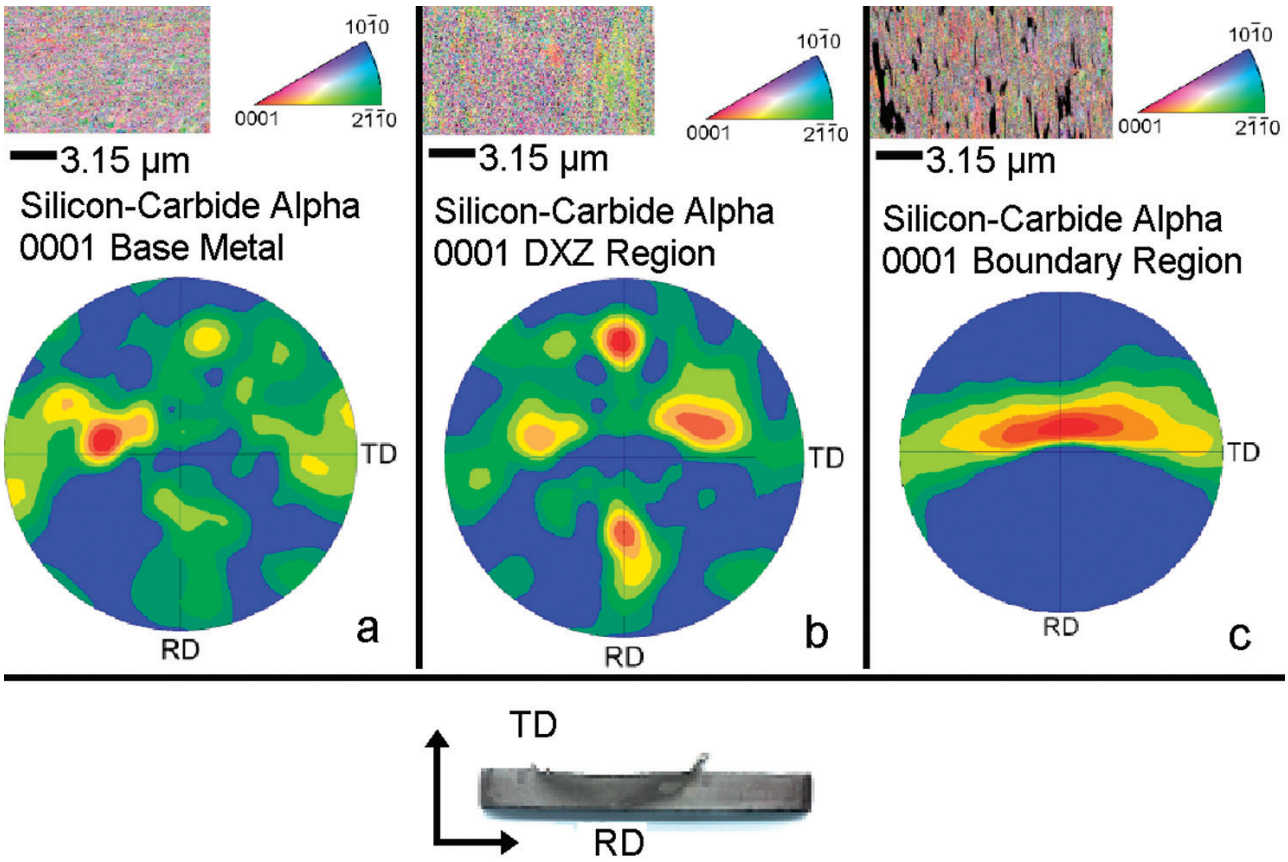

Fig. 9—Summary of the OIM, including images, inverse-pole-figure triangles (top), and {0001} texture maps (bottom) results from the hexagonal SiC crystal in (*a*) the BM, (*b*) the DXZ region, and (*c*) the boundary region between the TMAZ and DXZ regions. In the inset, the transverse and rolling directions are marked with respect to a macrostructure of the friction stir weld. The transverse direction (TD) corresponds to the *y* direction and rolling direction (RD) corresponds to the *x* direction shown in Figures 7 and 8. The red color in the texture image corresponds to a normalized peak value of 1; the blue color corresponds to a value of 0.

in the TMAZ and DXZ regions. This observation was further evaluated by performing image analyses of the optical micrographs, using a public domain ImageJ software[27] (Public Domain Free Software, National Institute of Health). The results (Table I) show that the average particle size decreased and the number of particles per unit area increased in the TMAZ and DXZ regions, in comparison to the BM and HAZ. The area distributions of the small particles are compared in Figure 13. The plots clearly show that the number of small particles increased in the TMAZ and DXZ regions. This result indirectly indicates that there is a tendency for Al_2O_3 particles to break up during FSW. This may be related to the coarseness of the initial Al_2O_3 particulates and the inability of these particles to reorient with the metal flow. Attempts to characterize the crystallographic orientation of these particles through OIM proved to be difficult, due to the poor diffraction quality. It is important to note that we could not identify the nature of these small particles; therefore, further work by TEM is necessary, to understand the constitution of these particles. Further work is also needed to determine the effect of such a breakup on the mechanical properties.

Recently, Lim *et al.*[28] have shown the coarsening and clustering of Mg_2Si particles in friction stir welds. Therefore, the interaction of Al_2O_3 on the stability of Mg_2Si requires further study. In a recent work, Wert[17] indicated the eutectic melting ahead of the tool due to overheating, in the case of an aluminum metal composite made up of a 2024 and a 2124 alloy reinforced with Al_2O_3, during friction stir joining. This phenomenon was deduced by the observation of the filmlike microstructure along the grain boundaries. In addition, Wert suggested that the particle strings and fragmentation of this eutectic microstructure also originate from these eutectic microstructures. Since we observed these small particles even in the low-temperature TMAZ regions, we speculate that the formations of these fine particles are mostly due to the breakup of the coarse Al_2O_3. However, we need further careful study to decouple the competing mechanisms of the eutectic melting and the fragmentation or breakage of coarse Al_2O_3 particles.

In case of Al-SiC composites, the SEM failed to show any breakage of the SiC whiskers. This may be due to the smaller size of these whiskers. The OIM analyses from these samples show that these whiskers have reoriented with the metal flow and, therefore, are not prone to breakage. The impact of the reorientation along the TMAZ and DXZ boundary on the mechanical properties needs to be evaluated in future research. The TEM (Figure 11) shows that the dislocation density was qualitatively higher in the DXZ regions than in the HAZ regions. This is also in agreement with the results by Fernandez and Murr.[15] It is well known that, due to differences in the thermal expansion between SiC and aluminum matrix, rapid heating and cooling will lead to

the generation of dislocations at the matrix-SiC interface.[29] The extent of the heating in the HAZ is lower than in the DXZ region; therefore, there is a reduced driving force available to generate dislocations in the matrix of the HAZ region.

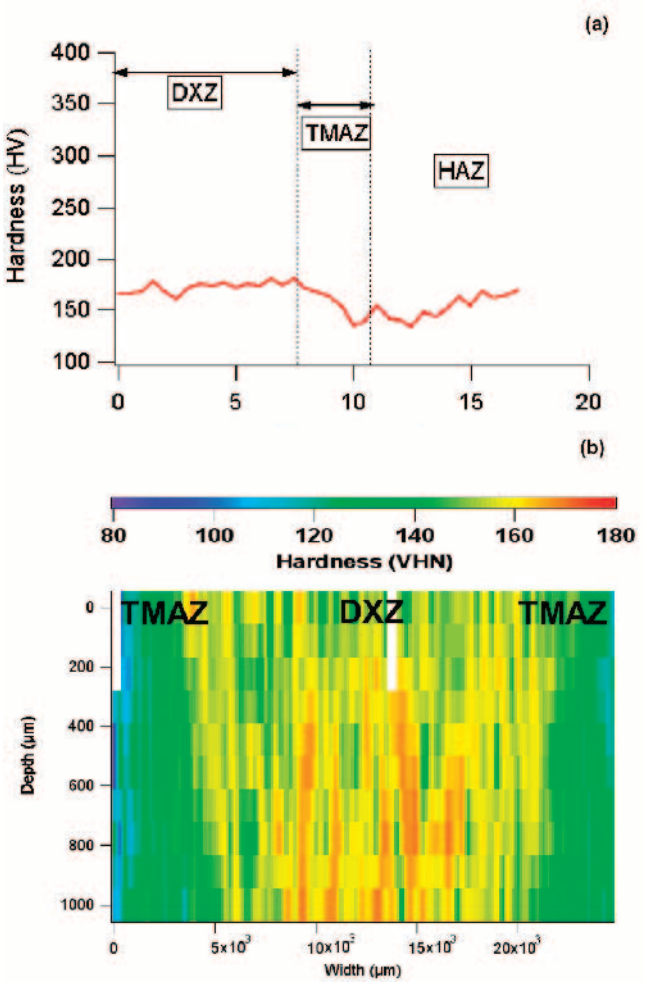

Fig. 10—(*a*) Measured hardness values as a function of distance from the center of the friction stir weld made on Al-SiC composites. (*b*) The spatial hardness distribution, measured across a larger area comprised of the DXZ and TMAZ regions, showing the presence of microstructural heterogeneity even within the DXZ.

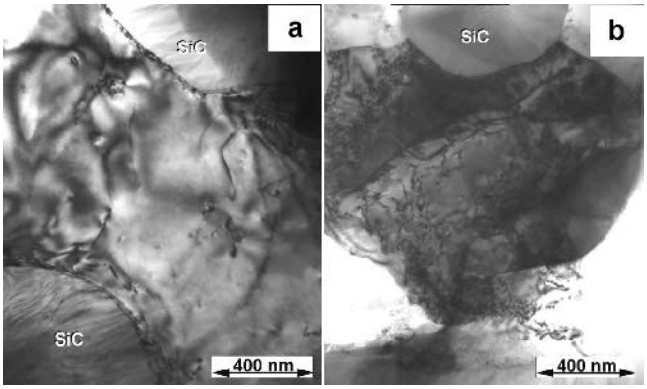

Fig. 11—(*a*) A transmission electron micrograph of the aluminum matrix in between two SiC whiskers from the HAZ shows fewer dislocations. (*b*) In contrast, a heavily dislocated matrix was observed in the DXZ region.

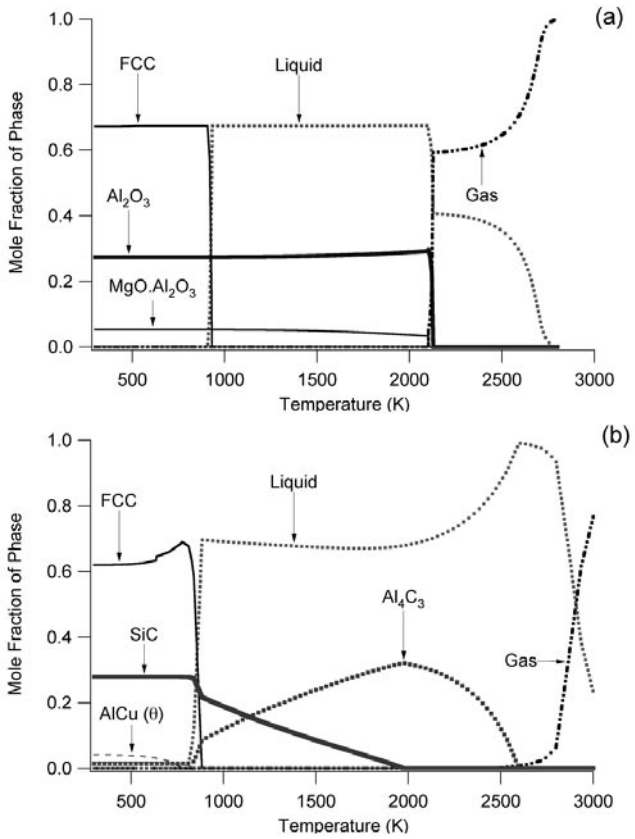

Fig. 12—(*a*) The calculated phase fraction as a function of temperature in (*a*) the Al-Al_2O_3 composite, and (*b*) Al-SiC composites.

Table I. Image Processing Results on Optical Micrographs from Al-Al_2O_3 Composites

Location	Number of Particles (μm^2)	Average Area (μm^2)	Area Fraction
BM	0.01	22	15 pct
HAZ	0.007	32	16 pct
TMAZ	0.039	7	18 pct
DXZ	0.025	8	14 pct

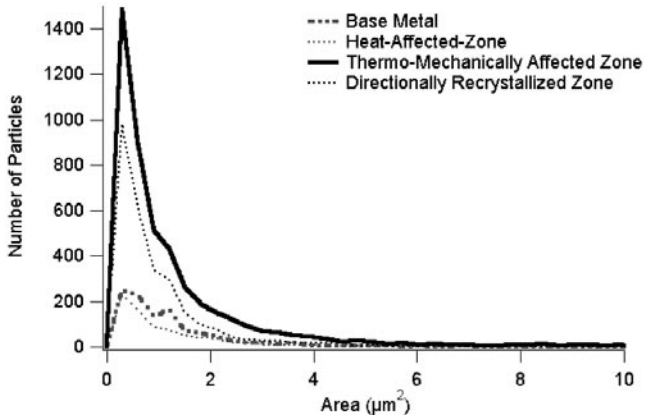

Fig. 13—Measured size distributions of small particles from the Al-Al_2O_3 composites from optical micrographs from the BM; the HAZ, TMAZ, and DXZ regions show an increase in the fraction of small particles in the TMAZ and DXZ regions.

Other mechanisms may also be responsible for the generation of dislocations in the DXZ region. In the past work, Ortelt *et al.*[30] observed that, within the DXZ region, one could observe a single grain with a high dislocation density being present very close to another grain with a recovered structure with low dislocation density. Therefore, the current results cannot delineate the possible mechanisms for the creation of a high number of dislocations in the matrix of the DXZ region. Further work is necessary to study the aluminum-metal-matrix composite with and without imposed thermomechanical strains.

VI. CONCLUSIONS

The tendencies toward the degradation of aluminum-metal-matrix composites by fusion-welding and FSW processes were investigated in Al6061-20 vol pct Al_2O_3 and Al2124-20 vol pct SiC whisker composites. Fusion welding could not produce successful welds with GTA, EB, and LB welding process in either composite.

During fusion welding of the Al-Al_2O_3 composites, the decomposition of Al_2O_3 occurred readily. This, in turn, led to very little weld-pool formation; this phenomenon was observed in GTA, LB, and EB welding processes. The removal of the Al_2O_3 reinforcement leads to a soft weld-metal region. In case of the Al-SiC composites, the fusion welding leads to rapid reaction of the SiC with the molten aluminum, and the formation of carbon compounds and Si-rich phases. The laser welding leads to deep keyhole-type weld penetration, in contrast to arc and EB welding processes, presumably due to the preferential absorption of the laser radiation by the SiC. The materials degradations during welding were calculated using thermodynamic models, and are in agreement with experimentally observed microstructures. The calculations suggested the control of peak temperature as the possible approach, to avoid the degradation of reinforcements in the aluminum-metal-matrix composites.

In contrast to the fusion-welding process, the FSW process led to good joints without much degradation of the microstructure in either composite. The FSW of Al-Al_2O_3 composites led to no discernable changes in the morphology or volume fraction of the Al_2O_3 reinforcement. There was some evidence for the breakage of the reinforcements during the FSW process. The hardness of the friction-stir-welded region was similar to that of the BM.

In the case of the Al-SiC whisker composites, the friction-stir-welded region shows a morphology similar to that of the SiC whisker distribution. However, very close to the boundary of the TMAZ and DXZ, the whiskers appear to align themselves in the welding direction. The OIM analysis from the BM and weld-metal regions shows a strong rod texture, due to the possible alignment of the SiC whiskers, along the major axes of their hexagonal crystal structure, with the welding direction. The hardness in the HAZ was slightly lower than that in the DXZ regions, due to differences in the dislocation density.

ACKNOWLEDGMENTS

The FSW and fusion-welding research was sponsored by the United States Department of Energy, Assistant Secretary for Energy Efficiency and Renewable Energy, Office of FreedomCAR and Vehicle Technologies (DSS, PSS, EE, and SAD), as part of the High Strength Weight Reduction Program. The modeling and characterization was sponsored by the Division of Materials Sciences and Engineering (SSB, OMB, and SAD), United States Department of Energy, under Contract DE-AC05-00OR22725, with UT-Battelle, LLC. The authors also thank Dr. B. Altshuller from ALCAN for providing the Al-Al_2O_3 composites. D. STORJOHANN thanks the Oak Ridge Associated Universities (ORAU) program for providing a summer internship at Oak Ridge National Laboratory. The authors thank Drs. Z. Feng and E. Ohriner for reviewing the manuscript.

REFERENCES

1. J.S. Ahearn, C. Cooke, and S.G. Fishman: *Met. Constr.*, 1982, vol. 14, pp. 192-97.
2. T. Iseki, T. Kameda and T. Maruyama: *J. Mater. Sci.*, 1984, vol. 19, pp. 1692-98.
3. C.D. Lundin, J.C. Danko, and C.J. Swindeman: *Proc. Int. Conf. on Recent Trends in Welding Science and Technology*, ASM INTERNATIONAL, Materials Park, OH, 1990, pp. 303-04.
4. N.B. Dahotre, M.H. McCay, T.D. McCay, S. Gopinathan, and L.F. Allard: *J. Mater. Res.*, 1991, vol. 6, pp. 514-29.
5. T.J. Linert, E.D. Brandon, and J.C. Lippold: *Scripta Metall. Mater.*, 1993, vol. 28, pp. 1341-46.
6. T.J. Linert and J.C. Lippold: Edison Welding Institute Report No. MR9403, Edison Welding Institute, Columbus, OH, May 1994.
7. K.U. Bhat and M.K. Surappa: *J. Mater. Sci.*, 2004, vol. 39, pp. 2795-99.
8. L.M. Liu, M.L. Zhu, D.S. Xu, and T. Wang: *Composite Interfaces*, 2002, vol. 9, pp. 135-42.
9. T.M. Yue, J.H. Du, and H.C. Man: *Mater. Sci. Technol.*, 1998, vol. 14, pp. 906-11.
10. C.B. Lin, C.K. Mu, W.W. Wu, and C.H. Hung: *Welding J.*, 1999, vol. 78, pp. 100s-108s.
11. M.J. Cola, G.S. Martin, and C.E. Albright: Edison Welding Institute Report No. MR9108, Edison Welding Institute, Columbus, OH, 1991.
12. J.C. Devletian: *Welding J.*, 1987, vol. 66, pp. 33-39.
13. M.B.D. Ellis, M.F. Gittos, and P.L. Threadgill: The Welding Institute Report No. 501/1994, The Welding Institute, Cambridge, UK, 1994.
14. R.S. Mishra, Z.Y. Ma, and I. Charit: *Mater. Sci. Eng.*, 2003, vol. A341, pp. 307-10.
15. G.J. Fernandez and L.E. Murr: *Mater. Characterization*, 2004, vol. 52, pp. 65-75.
16. R.A. Prado, L.E. Murr, D.J. Shindo, and K.F. Soto: *Scripta Mater.*, 2001, vol. 45, pp. 75-80.
17. J.A. Wert: *Scripta Mater.*, 2003, vol. 49, pp. 607-12.
18. K. Nakata, S. Inoki, Y. Nagano, and M. Ushio: *Mater. Sci. Forum*, 2003, vols. 426–432, pp. 2873-78
19. J.O. Andersson, T. Helander, L. Hoglund, and B. Sundman: *CALPHAD*, 2002, vol. 26, pp. 273-312
20. *SGTE, 2002*, SSOL2-SGTE Solutions Database, Version 2.0 (provided by ThermoCalc software, Stockholm, Sweden).
21. *SGTE, 1996*, The SGTE Casebook: Thermodynamics at Work, K. Hack, ed., Institute of Materials, London, pp. 227-30.
22. O.M. Barabash, S.S. Babu, J.M. Vitek, J.W. Park, J.A. Horton, G.E. Ice, and R.I. Barabash: *J. Appl. Phys.*, 2004, vol. 96, pp. 3673-79.
23. O.M. Barabash, S.S. Babu, J.M. Vitek, and R.I. Barabash: *J. Appl. Phys.*, 2003, vol. 94, pp. 738-42.
24. *Welding Handbook*, vol. 2, *Welding Processes*, 8th ed., American Welding Society, Miami, FL, 1992, p. 672.
25. Q.J. Zheng and R.G. Reddy: *High Temp. Mater. Processes*, 2003, vol. 22, pp. 35-45.
26. J.-C. Lee, J.-P. Ahn, Z. Shi, J.-H. Shim, and H.-I. Lee: *Metall. Mater. Trans. A*, 2001, vol. 32A, pp. 1541-50.
27. ImageJ Public domain Java Image processing program, http://rsb.info.nih.gov/ij/docs/intro.html
28. S. Lim, S. Kim, C.-G. Lee, and S. Kim: *Metall. Mater. Trans. A*, 2004, vol. 35A, pp. 2829-35.
29. R.J. Arsenault and N. Shi: *Mater. Sci. Eng.*, 1986, vol. 81, pp. 175-87.
30. G. Oertelt, S.S. Babu, S.A. David, and E.A. Kenik: *Welding J.*, 2001, vol. 80, pp. 71s-79s.